REFERENCE 148

J. E. SCHWAGER, F. A. KLOVERSTROM, AND W. S. GILBERT, "CRITICAL MEASUREMENTS ON INTERMEDIATE-ENERGY GRAPHITE-U^{235} SYSTEMS," UNIVERSITY OF CALIFORNIA RADIATION LABORATORY REPORT UCRL-5006 (NOVEMBER 1957).

UCRL-5006

UNIVERSITY OF CALIFORNIA
Radiation Laboratory, Livermore Site
Livermore, California

Contract No. W-7405-eng-48

CRITICAL MEASUREMENTS ON INTERMEDIATE-ENERGY GRAPHITE-U^{235} SYSTEMS

J. E. Schwager,* F. A. Kloverstrom, and W. S. Gilbert

November 15, 1957

*Lieutenant Commander, U. S. Navy, on special assignment.

Printed for the U.S. Atomic Energy Commission

CRITICAL MEASUREMENTS ON INTERMEDIATE-ENERGY GRAPHITE-U^{235} SYSTEMS

J. E. Schwager, F. A. Kloverstrom, and W. S. Gilbert
University of California Radiation Laboratory
Livermore Site

November 15, 1957

ABSTRACT

A system for the measurement of near-homogeneous carbon-U^{235} critical masses is described. Cores are constructed with thin, enriched-uranium foils spaced between graphite blocks. Fuel density is variable by use of different foil thicknesses and spacings. Reactivity is controlled by boron rods; standard reactor instrumentation permits critical operation at low power. Results of critical measurements on unreflected systems having atomic C/U^{235} ratios of 670, 1380, and 2590 are given. Thin reflectors of graphite and beryllium were also used. Corrections for self-shielding in the fuel foils and systematic errors are described.

UCRL-5006
Internal

CRITICAL MEASUREMENTS ON INTERMEDIATE-ENERGY GRAPHITE-U^{235} SYSTEMS

J. E. Schwager, F. A. Kloverstrom, and W. S. Gilbert
University of California Radiation Laboratory
Livermore Site

November 15, 1957

I. INTRODUCTION

Critical-mass, zero-power flux measurements have been made on a variety of bare and reflected carbon-uranium reactors. Graphite and uranium components were designed to approximate a homogeneous system. The systems were controlled exclusively with nuclear poisons. A simple and versatile design resulted from eliminating the conventional moving-table assembly machine. This simplification also minimized extraneous support masses in and around the core, thus reducing perturbations from unwanted absorptions and reflections. To provide flexibility for studying various geometries and carbon-to-U^{235} ratios, thin graphite plates and separate Oy fuel foils were used for core material. Briefly then, the apparatus was a compact control unit supported over a low-mass aluminum table. A reactor was assembled by stacking graphite-uranium foil sandwiches around the control unit.

II. DETAILED DESCRIPTION

A. Low-Mass Table

The low-mass stacking table (Fig. 1) upon which the reactors were assembled consists of an 8' x 8' x 1' aluminum honeycomb slab, rigidly supported by an aluminum stand. The honeycomb is made of 2-mil 2S aluminum foil in a 3/8" hexagonal cell lattice with a density of 3 lb/ft^3. Table height is 4 ft off the floor, thus reducing floor reflection and providing ample space for the installation of neutron detectors and accessory equipment beneath the table. Neutronically speaking, measurements were made on levitated systems.

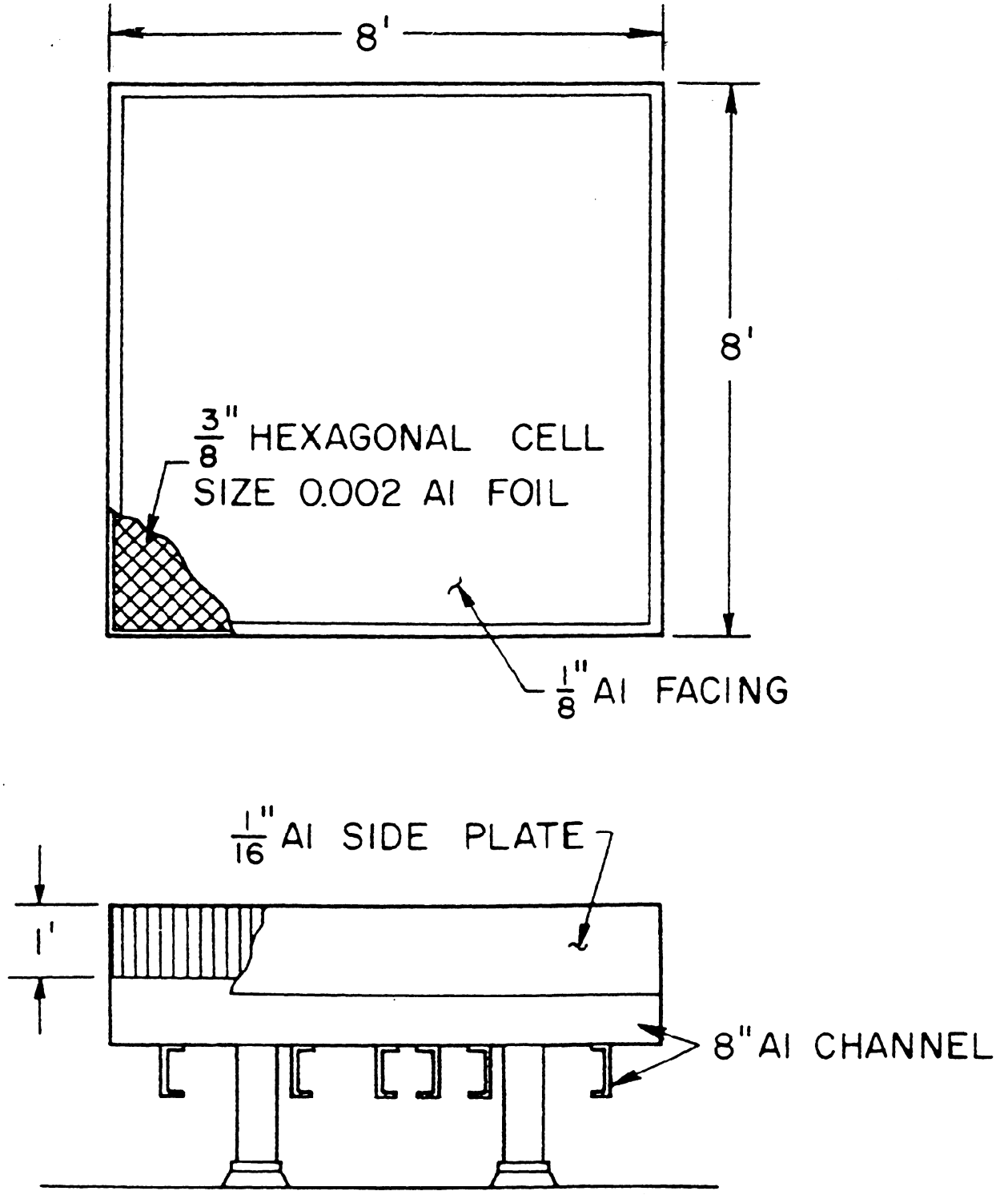

Fig. 1. Low-mass table.

B. Control System

A braced post-and-beam aluminum frame rigidly suspends the control unit over the low mass table. The control unit is a 2S aluminum canister (Fig. 2) with 4 channels in X-cross section (each 1/2" x 6" exterior dimension) mounted beneath a manual-electric drive assembly. Each channel guides a 1/4"-thick, 4'-long boral element (boral is a fabricated material consisting of boron sandwiched between two slices of aluminum). Three of the elements (5" wide) are safety rods and the fourth (1" wide) is the control rod. A tube through the canister axis permits insertion of various sources into the core.

All three safety rods are lifted by electromagnets suspended by cables from the top of the unit, the magnets being de-energized for gravity-drop scram. Scram time is 0.65 sec for 4 foot drop, including ±0.06-sec magnet delay. Highly damped shock absorbers minimize bouncing of scrammed elements. Two of the safety rods are lifted manually and the third has an electric drive. The magnet for the electrically driven safety rod is lifted at 4.8 inches/minute and lowered at 4 feet/minute. In contrast, the control rod is moved by an electrically driven jack screw which provides rates of 1 inch/minute and 10 inches/minute for both insertion and extraction.

C. Materials

A selection of nominally 1- and 2-mil-thick Oy foils (93-1/2% U^{235}) in 5-1/4" x 5-1/4" squares and isosceles triangles was used for fuel. All foils were coated with a fluorocarbon plastic (Teflon — see Table I for analysis) to prevent oxidation and reduce erosion, there being an average of 0.920 grams of plastic per 2-mil-square foil. The fuel foils have a normal average surface reading of 3/4 mr/hr gamma and 10 mr/hr beta. Surgical gloves were worn whenever the fuel foils were handled and they reduced beta levels by a factor of 10.

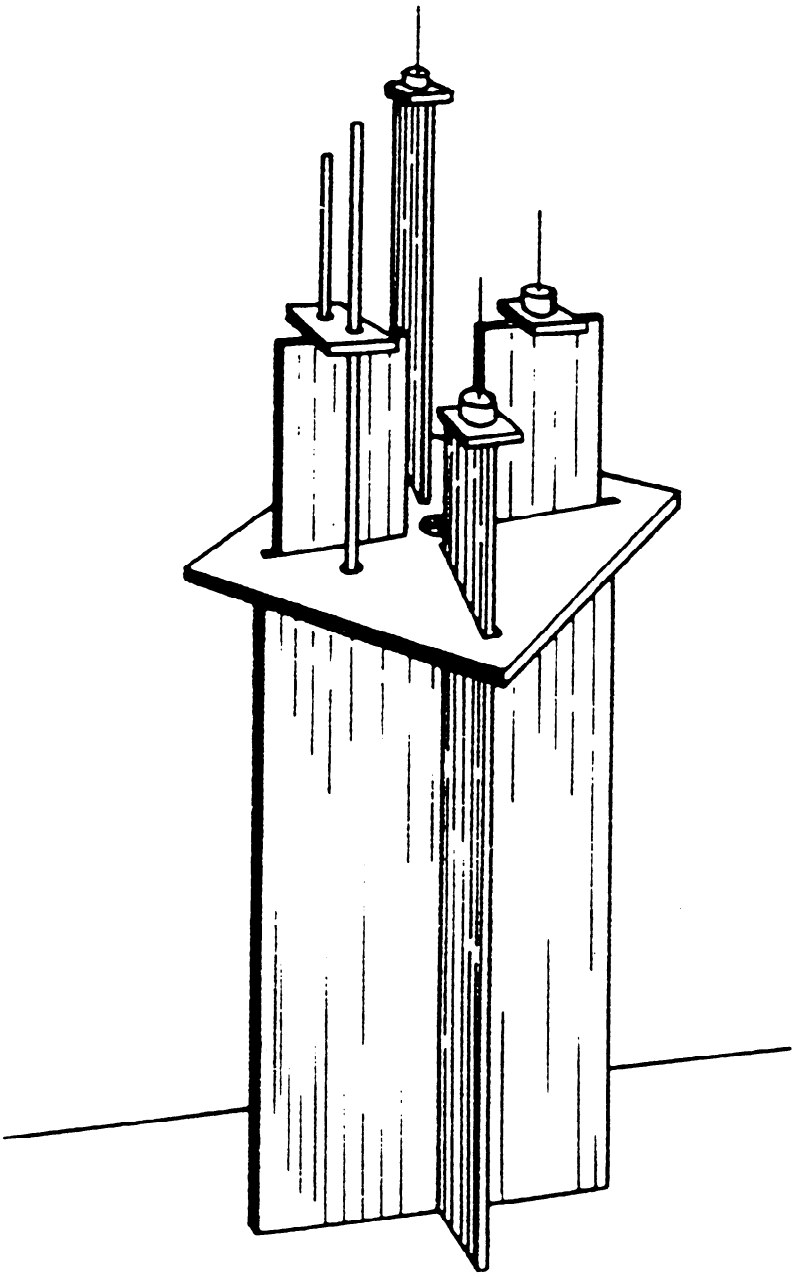

Fig. 2. Control and safety-rod assembly.

Table I. Analysis of Teflon.

$(CF_2)_n$ Density = 2.1 g/cc

Less than one part per million of:	Al, Ca, Co, Cr, Cu, Fe, Mg, Mn, Mo, Ni, Si, Sn.
No proton signal from magnetic resonance test. This indicates less than three parts per thousand hydrogen.	

Table II. Analysis of ATJ Graphite.

Density = 1.73 g/cc

Element	Parts per million
B	14.4
Ca	200
Al	200
Mg	30
Fe	600
Ag	6
Cu	500
Ti	60

Core material is ATJ graphite (see Table II for analysis) machined in 1/2" thick, 6" x 6" solid and grooved squares and triangles with a 10-mil recess milled in the top to accommodate the fuel foils (see Figs. 3 and 4.). The grooved graphite plates had a 40% void volume and were used as pallets for rapid core operations. Units of graphite plates with sandwiched fuel foils were prestacked on the graphite pallets up to 6" high and were readily lifted into core position with a small hand fork. A core lattice of one 2-mil fuel foil on top of each graphite plate gave a nominal absolute atomic carbon-to-U^{235} ratio of 600/1.

ATJ graphite core material and standard production QMV solid beryllium were used for reflector material on the reflected systems. The beryllium has a density of 1.84 g/cm^3 and has been machined into a selection of convenient-size parallelepipeds for easy handling and versatility.

Systems were built up by hand on the low-mass table around the control unit canister (Fig. 5). The canister created a void with 12-1/4 in^2 cross section throughout the core length, and nonporous graphite plates were placed on end to plug the canister extension to core edge. Graphite-plugged channels were constructed as the assembly proceeded, thus affording easy access to the core interior for later flux studies. A simple banding system constrained the reactor and tied it to the control unit through peripheral tension. One band at the top provided ample stability.

D. Neutron Sources

Two Po-Be neutron sources were used. Each was insertable through a tube (mounted along the control canister axis) to a point 20" from the core bottom (Fig. 6).

One of the sources had a strength of 10^7 neutrons/sec and was manually operated from the control room by a pulley system lifting from above the core. It was used to take base rates and to drive the assembly at low multiplications. During loading operations (or other occasions when this source was not desired in the core) it was withdrawn to a position on top of the vault ceiling timbers.

The second source had a strength of 10^5 neutrons/sec and was normally nested in the core. It must occupy this position to allow personnel entry into the vault and to withdraw the safety and the control rods. The withdrawal of the source is a positive test for criticality. It is also removed when the assembly is run as a reactor for flux or irradiation

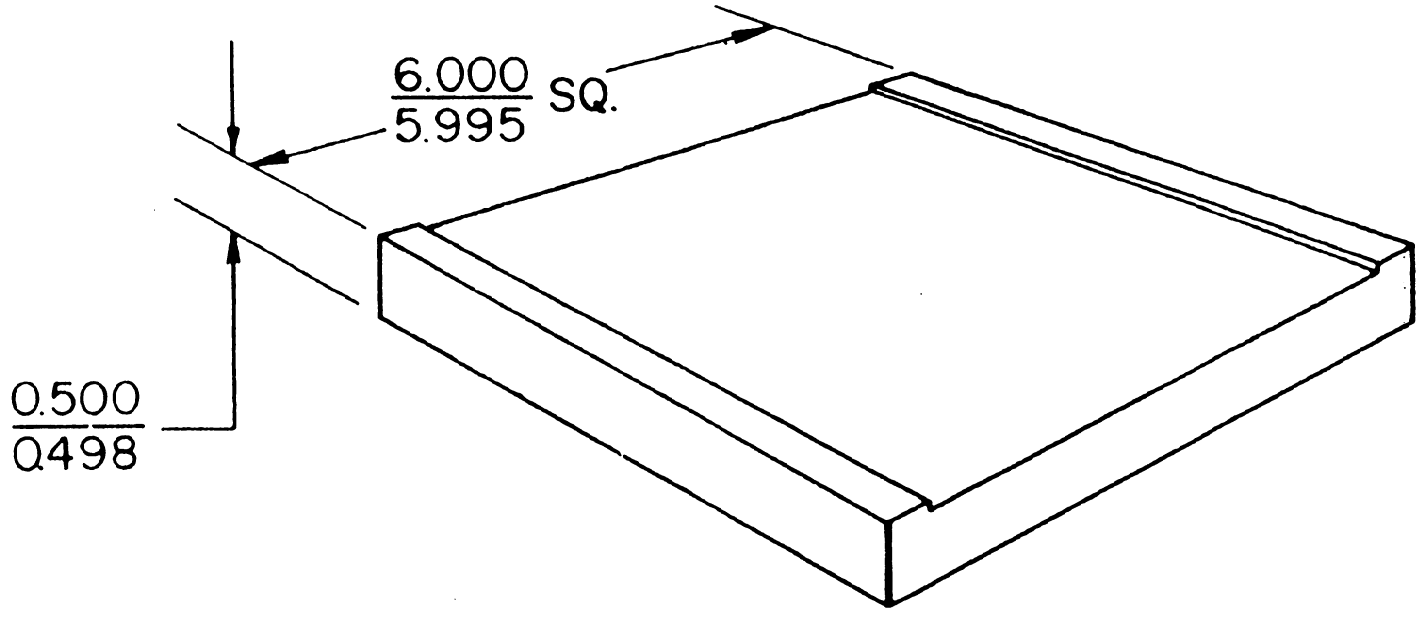

Fig. 3. Full block.

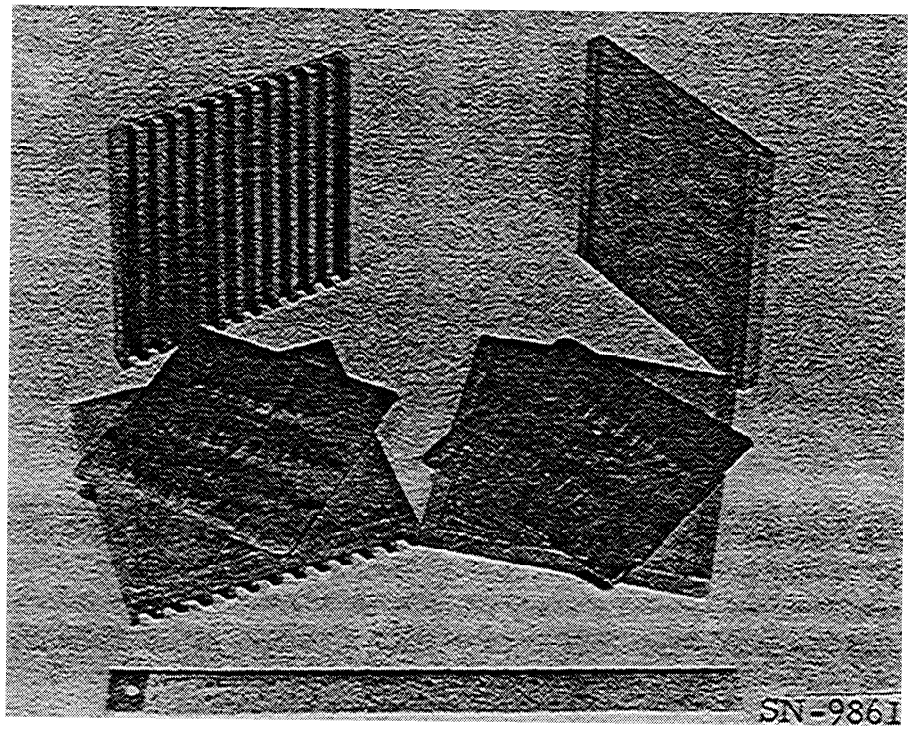

Fig. 4. Core material.

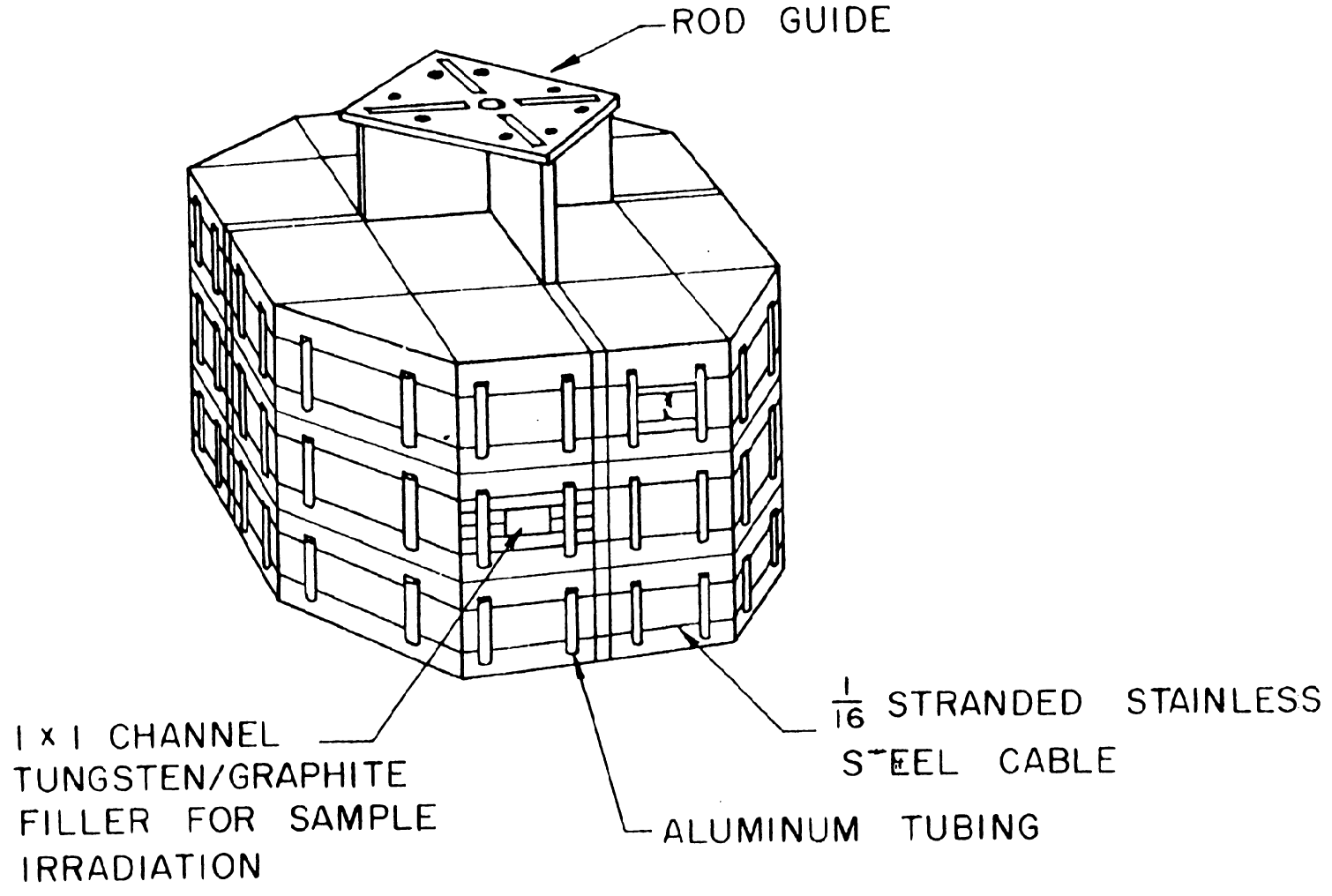

Fig. 5. Core and restraint.

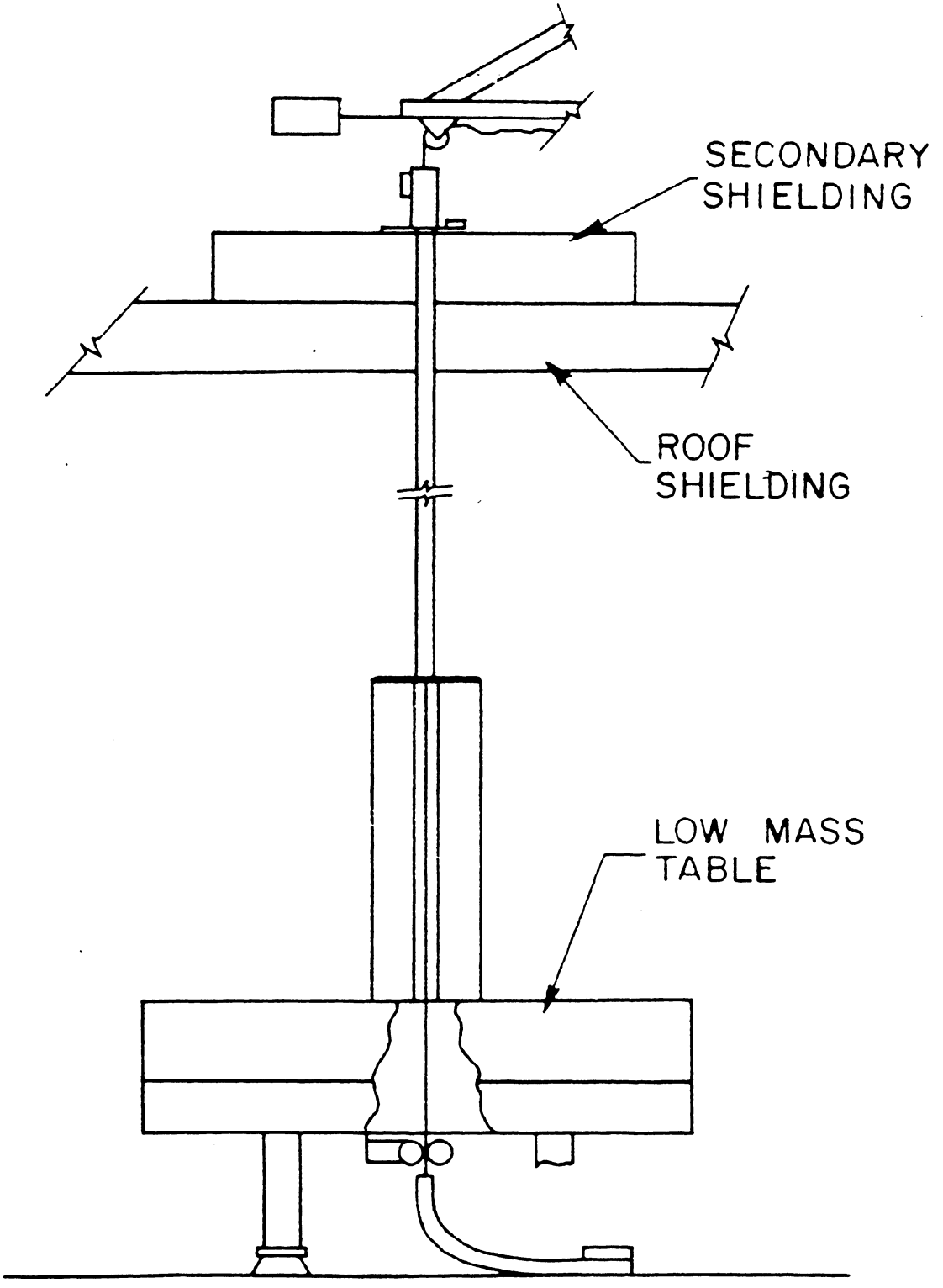

Fig. 6. Neutron source system.

studies. The withdrawal is accomplished by an electrically operated mechanism, mounted beneath the low-mass table, which pushes the source out the top of the core for extraction. This provision is necessary because neutron detectors are installed beneath the low-mass table and false readings would result from lowering the source for removal.

E. Paraffin Slab

The pseudo-octagonal and the parallelepiped geometries are shown assembled in Figs. 7 and 8, respectively. The object on the left in Fig. 8 is a movable paraffin slab. A complication in performing unreflected assemblies is body reflection, since the bodies of personnel working on the core reflect neutrons and increase the core reactivity. This generates a potentially dangerous situation as criticality is approached because body reflection may increase reactivity beyond the control of the safety rods and drive the assembly critical during loading operations.

The paraffin slab suspended from rails and electrically operated from the control room was used to assure that a contemplated manual change in core loading could be accomplished safely. This was predicted by extrapolating a series of measurements taken with the paraffin slab against the core while the safety rods were in the loading configuration. The slab was 4' high by 2' wide by 6" thick and was mounted with the 2' x 4' surface parallel to the core face. It was wired into the safety chain so that it positively could not be used as a reactor control, and a manually inserted locking pin mechanically locked the slab carriage in the fully retracted position when the vault was occupied. As a further precaution, one of the three safety rods was always withdrawn and kept cocked for scram by a vault monitor chain during loading operations.

F. Instrumentation

At low multiplications the assembly was driven by the 10^7 n/sec Po-Be source. Since power levels of a few watts were used for irradiation studies, there were 10^{11} fissions/sec occurring in the core during irradiation. A range of about 10^4 must be covered by the detectors. Several different types of detectors were used to give adequate coverage over this range.

Two types of neutron detectors were used for the lowest flux levels: LiI (Eu) scintillation detectors and a Hanson-McKibben long counter, each with an amplifier-scaler and count-rate meter. The scintillation detector-count rate meters were sensitive down to approximately 10 n/cm^2/sec and

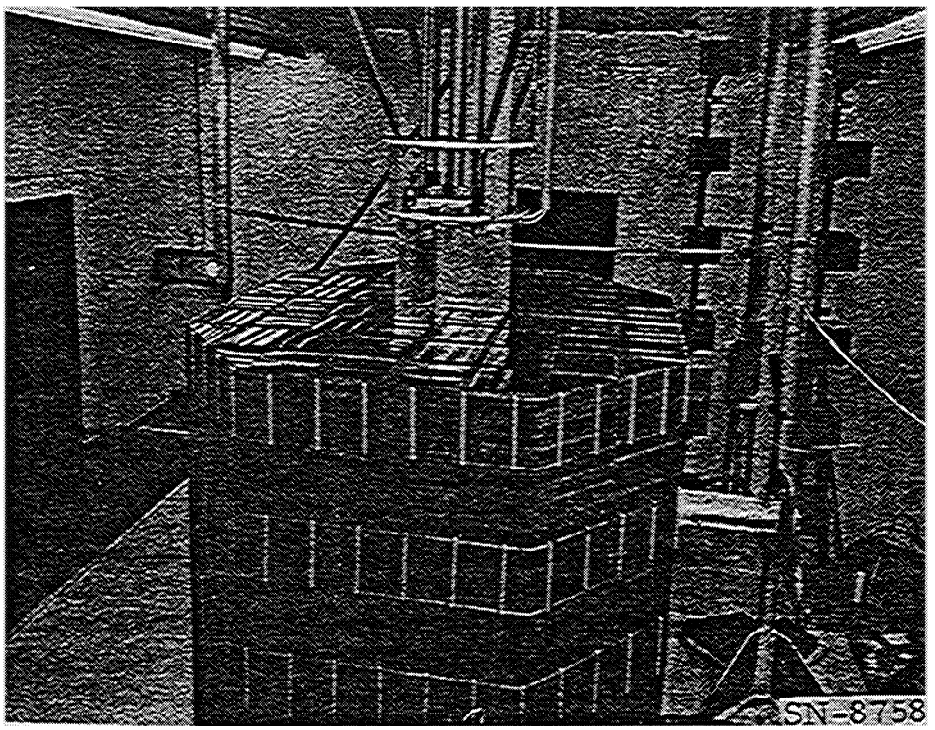

Fig. 7. Pseudo-octagonal configuration.

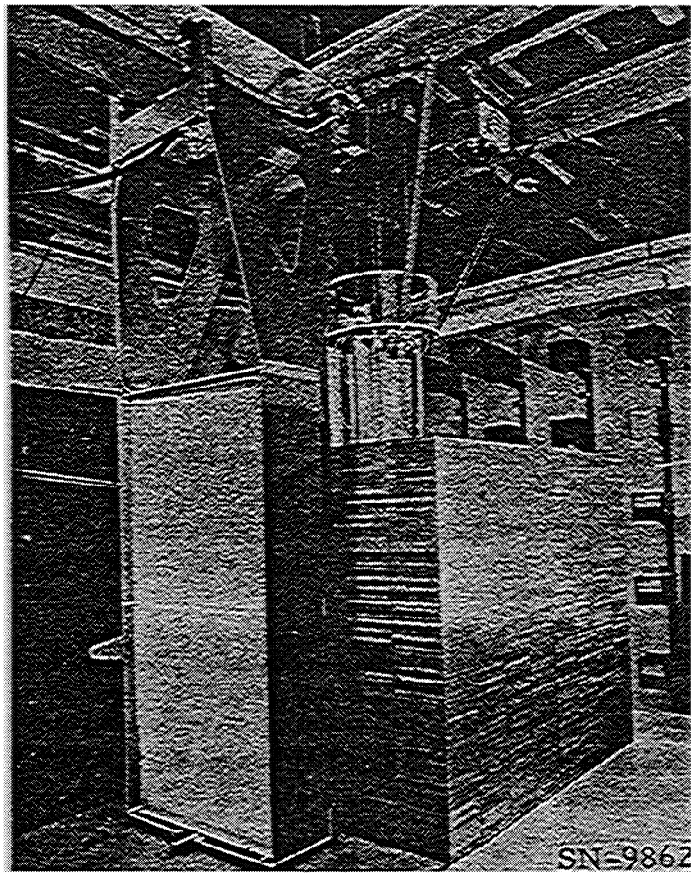

Fig. 8. The parallelepiped geometry with paraffin slab advanced.

had a 4-decade range. The Hanson counter covers the range of 10-10^4 $n/cm^2/sec$.

Two Beckman micro-microammeters were employed. Each had a six-decade range and a time constant varying between 0.12 and 1 second, depending on the range. A BF_3 ionization chamber was used with a Beckman meter No. 1, and covered a range from 10^2-10^8 $n/cm^2/sec$. For higher levels a boron-lined ionization chamber drove a Beckman meter No. 2 to cover a range from 10^4-10^{10} $n/cm^2/sec$. Each micro-microammeter had its own recording potentiometer which gave a continuous record of the neutron flux level.

Another BF_3 ionization chamber operated a log n amplifier, a reactor period meter (response time: 1/2 sec above 10^3 $n/cm^2/sec$), and a recording potentiometer. This logarithmic monitor covered the range from 10^2 to 10^7 $n/cm^2/sec$. At low flux levels (10 to 3 x 10^3 $n/cm^2/sec$) the reactor period was monitored by a period meter utilizing the log scale of the scintillation detector-count rate meter. The time constant of this meter was 1 sec in this range and shorter for higher ranges.

All of these neutron detectors were in the safety chain, hence a high flux level would scram both the linear and the log n detectors; a fast reactor period would scram the log n-period meter and the scintillation detector-period meter. By providing at least three independent neutron flux monitors and two reactor period meters, the possiblility of an electronic failure affecting the safety of the assembly was greatly reduced.

A remote-recording area-survey monitor was also installed in the experimental facility to monitor gamma flux levels during and after operation. This instrument had a range from 10 mr/hr to 100 r/hr.

G. Installation

The photographs (Figs. 4 and 7) show how completely accessible the reactors are and reveal how relatively remote an assembly is from the vault concrete surfaces. The timbered ceiling is 12-1/2 feet high and the nearest wall is 10 feet away from the control-unit axis.

III. OPERATION

The first step in making a critical assembly was to take base rates on an inert core. Graphite alone was stacked in the desir d core geometry

and counting rate vs core height were run on each of the counters with both Po-Be neutron sources nesting in the core position. The table was then cleared and the assembly begun. A series of counting rates vs core-height measurements were then taken as the uranium-graphite core was built up. A multiplication was defined for a given instrument and core height by taking the ratio of fertile to inert core counting rates. Obviously this was not the true multiplication of the system, but this is of no consequence. It was only important that counters agree that the multiplication was infinite at critical.

As criticality becomes imminent, the last nuclear-poison elements removed from the assembly assume an obvious importance. If the assembly has potential excess reactivity and the multiplication is increased at too fast a rate during rod removal, criticality could be reached and the reactor driven to a dangerously-high energy level before scrams are able to shut the system down. Theoretical studies indicated that in case of operator error, the following restrictions on the assemblies should provide shutdown with a satisfactory margin before prompt critical and with only innocuous amounts of energy released:

1. Maximum rod dk/dt: 0.05% reactivity/sec
2. Scram signals set for:
   a. less than 1.5-watt power level
   b. greater than +5 sec period
3. Scram interval: 1 second.

Because of its enforced slow withdrawal rate, the electrically operated safety rod could be worth up to 20% reactivity and still not allow a rod-induced accident to become dangerous if it should occur. A sequencing arrangement assures that this safety rod would be the last safety rod withdrawn, since power for full extraction is not available to its motor drive unless the two manual rods are fully removed. Similarly, the control rod cannot be withdrawn unless all three safety rods are pulled. It is possible, however, to lift the control rod and the electrically driven safety rod just off their respective bottom microswitches with the manual rods inserted, so that these elements can be scram-tested.

Five control conditions were defined as follows:

Condition	SR No. 1	Paraffin Slab	SR No. 2	SR No. 3	Control Rod
2	Out	In	In	In	In
1	Out	Out	In	In	In
3	Out	Out	Out	In	In
4	Out	Out	Out	Out	In
5	Out	Out	Out	Out	Out

Curves of inverse multiplication vs core height for each of the above control conditions were plotted for an assembly from a series of counting-rate measurements beginning with a core height definitely known to be subcritical. Extrapolation of the various curves predicted a critical height for the respective control configurations and showed the amount by which the core height could be safely increased for the next measurement. In this way, the core was built up in successively safe increments until criticality was reached.

Figure 9 shows plots of inverse multiplication vs core height obtained with one of the counters for the various control conditions during the assembly of a pseudo-octagonal core (Assembly No. 1 of Table III). Using the extrapolations to critical, the worth of the various elements in terms of core height is: control rod = $0.3^{+''}$, one safety rod = 1.6", 2 safety rods = 3.0", and the paraffin slab = 0.7". This is for the case of C/U = 600/1. For more dilute loadings the worth of the rods is increased.

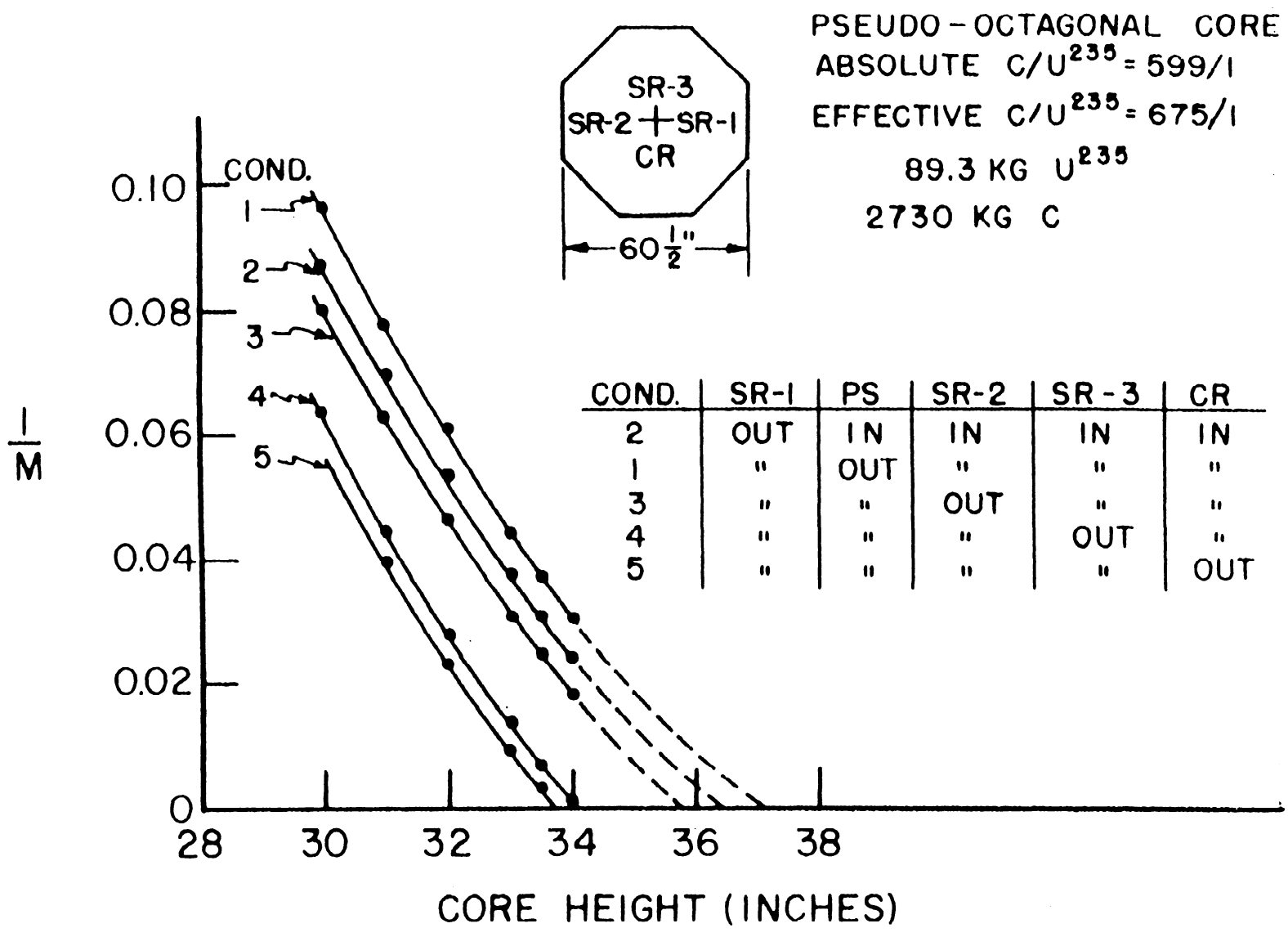

COND.	SR-1	PS	SR-2	SR-3	CR
2	OUT	IN	IN	IN	IN
1	"	OUT	"	"	"
3	"	"	OUT	"	"
4	"	"	"	OUT	"
5	"	"	"	"	OUT

Fig. 9. Inverse multiplication curves for Critical Assembly No. 1.

IV. CRITICAL MASS DATA

Figure 10 shows appropriately labeled dimensions for the octagonal and rectangular core geometries. Corresponding core and reflector dimensions are given in Table III.

Table III lists all the critical mass data. Following Table III are notes giving further data on the lattices used and the remarks pertinent to some of the experiments.

Table IV is a summary of the critical-mass data for the basic systems. This table contains data abstracted from Table III.

Table IV. Summary of Critical-Mass Data for the Basic Systems.

Core Size (inches)	Reflector Thickness (inches)	C/U Absol.	C/U Eff.	H_c (inches)	U^{235} (kg)	
60-1/2 octag.	0	600	675	33.8	89.3	Pseudo Octagon
54-1/2 "	0	600	675	38.8	79.1	
48-1/2 "	0	600	675	42.3	76.5	
42-1/2 "	0			~61	~112	
36-1/2 "	~6-C-8 sides	600		44.3	40.5	
48-1/2 x 48-1/2	0	600	675	40.0	82.3	
48-1/2 x 48-1/2	0	1200	1379	42.4	43.5	
48-1/2 x 36-1/2	6-C-2 sides	1200		42.8	33.0	X off center
36-1/2 x 36-1/2	6-C-4 sides	1200		43.5	25.3	X $6\sqrt{2}$ off center diagonally
48-1/2 x 48-1/2	0	2340	2586	47.6	25.1	
48-1/2 x 36-1/2	6-Be-2 sides	2340		40.9	16.2	X 6" off center
36-1/2 x 36-1/2	6-Be-4 sides	2340		36.8	11.0	X 6" off center

Table III. Critical Mass Data.

(Explanatory Notes appear on following pages.)

Assembly No.	Geometry	Reflector	Dimensions (inches) a	a'	b	b'	c	c'	d	e	Lattice	Critical Height (inches)	Critical Mass (kg) Core C	U^{235}	Core Al	Reflector	C/U^{235} Absolute	Effective	Remarks
1	A	*	60-1/2	*	24-1/2	*	25.5	*	30-1/4	30-1/4	a	33.8	2730	89.3	6.04	*	599	675	
2	"	"	54-1/2	"	18-1/2	*	"	"	24-1/4	24-1/4	"	38.8	2420	79.1	6.94	"	"	"	
3	"	"	48-1/2	"	24-1/2	"	17.0	"	"	"	"	42.3	2340	76.5	7.48	"	"	"	
4	"	"	42-1/2	"	18-1/2	"	"	"	18-1/4	18-1/4	"	(61)	(3430)	(112)	(10.9)	"	"	"	
5	"	C	36-1/2	48-1/2	12-1/2	24-1/2	"	17.0	"	"	"	44.3	1240	40.5	7.91	1210	"	+	
6	B	*	48-1/2	*	48-1/2	*	*	*	24-1/4	24-1/4	b	40.0	2520	82.3	7.15	*	600	675	
7	"	"	"	"	"	"	"	"	"	"	c	42.3	2670	43.5	3.85	"	1200	1379	
8	"	"	"	"	"	"	"	"	"	"	d	42.3	"	43.6	3.86	"	"	"	II
9	"	"	"	"	"	"	"	"	"	"	c	42.5	2660	43.4	3.84	"	"	"	III
10	"	"	"	"	"	"	6.0	"	"	"	"	42.9	2690	44.1	3.90	"	"	"	IV
11	"	"	"	"	"	"	*	"	"	36-1/4	"	41.8	2640	43.1	3.81	"	"	"	V
12	"	"	"	"	"	"	"	"	"	42-1/4	"	41.4	2610	42.5	3.76	"	"	"	VI
13	"	"	"	"	"	"	24.0	"	"	"	"	42.3	2650	43.4	3.84	"	"	"	VII
14	"	"	"	"	"	"	"	"	"	"	"	42.5	2660	43.6	3.85	"	"	"	VIII
15	"	"	"	"	"	"	"	"	"	"	"	43.3	2730	44.5	3.90	"	"	"	IX
16	"	"	"	"	"	"	"	"	"	"	"	44.8	2880	46.1	4.08	"	"	"	X
17	"	C	"	0	36-1/2	6.0	*	"	12-1/4	36-1/4	"	42.7	2030	33.0	3.88	667	"	+	XI
18	B	C	36-1/2	6.0	36-1/2	6.0	*	*	12-1/4	24-1/4	c	43.5	1550	25.3	3.95	1190	1200	+	XII

Table III. (Contd.)

Assembly No.	Geometry	Reflector	Dimensions (inches) a	a'	b	b'	c	c'	d	e	Lattice	Critical Height (inches)	Critical Mass (kg) Core C	U^{235}	Core Al	Reflector	C/U^{235} Absolute	Effective	Remarks
19	"	*	48-1/2	*	48-1/2	*	"	"	24-1/4	"	"	47.6	3000	25.1	4.33	*	240	286	
20	"	"	"	"	"	"	"	"	"	36-1/4	"	46.8	2960	24.7	4.26	"	"	"	V
21	"	"	"	"	"	"	"	"	"	42-1/4	"	46.4	2930	24.5	4.21	"	"	"	VI
22	"	"	"	"	"	"	6.0	"	"	"	"	46.9	2950	24.7	4.26	"	"	"	VII
23	"	Be	"	0	36-1/2	3.0	*	"	18-1/4	30-1/4	"	48.1	2280	19.1	4.37	422	"	+	XI
24	"	"	"	"	"	6.0	"	"	"	"	"	40.9	1940	16.2	3.72	717	"	+	"
25	"	"	36-1/2	6.0	"	"	"	"	"	24-1/4	"	36.8	1320	11.0	3.34	1130	"	+	XII
33	"	*	48-1/2	*	48-1/2	*	"	"	24-1/4	"	"	47.8	3010	25.2	4.33	*	240	286	III

* Not applicable

+ Undetermined

( ) Gross extrapolation

Notes Pertaining To Table III

Lattice

a. All core columns are constructed with one 2-mil Oy fuel foil recessed on top of each 1/2" thick ATJ graphite plate. The graphite plates are stacked with one 0.4 porosity plate (av. density = 1.03 g/cm^3) beneath eleven nonporous plates (av. density = 1.70 g/cm^3) beginning with a porous plate at the bottom.

Control system void/inch of core height	= 12-1/4 $in^3/in.$
Control system aluminum/inch of core height	= 179 g/in.
Av. core porosity (excluding control void)	= 0.050
Over-all graphite density (excluding control void)	= 1.645 g/cm^3
Over-all U^{235} density	= 0.05345 g/cm^3
Over-all $(CF_2)_n$ density	= 0.0031 g/cm^3

b. Same as "a" except that over-all U^{235} density = 0.05334 g/cm^3

c. Same as "a" except for:
One 2-mil Oy fuel foil recessed on top of every other 1/2"-thick graphite plate beginning with the bottom plate.

Control system aluminum/inch of core height	= 91.0 g/in.
Over-all U^{235} density	= 0.02667 g/cm^3
Over-all $(CF_2)_n$ density	= 0.0015 g/cm^3

d. Same as "c" except that porous plates are randomized in position and orientation.

e. Same as "a" except for:
One 1-mil Oy fuel foil recessed on top of every other 1/2" thick graphite plate beginning with the bottom plate.

Control system aluminum/inch of core height	= 91.0 g/in.
Over-all U^{235} density	= 0.01369 g/cm^3
Over-all $(CF_2)_n$ density	= 0.0011 g/cm^3

Notes Pertaining To Table III (Continued)

Remarks (See last column of Table III)

I. No end reflectors.

II. Test for neutron streaming through, and density inhomogeneity from, porous plate grooves. Effect negligible.

III. Test for thermal neutron reflection from vault. Entire core surrounded with 1/4" thick boral sheet.

IV. Control system void axis aligned with core axis and a 1/2" x 12" cross-sectional test void installed as indicated by dimension "c".

V. Control system void axis displaced 12" from core axis. No test void.

VI. Control system void axis displaced 18" from core axis. No test void.

VII. Control system void axis displaced 18" from core axis and a 1/2"x 12" cross-sectional test void installed as indicated by dimension "c".

VIII. Test for core poisoning by control-system aluminum. Remark VII with test void filled with aluminum (11.3 kg).

IX. Investigate potentiality of Cd control in low epithermal systems. Remark VII with a 0.030" thick, 1" x 4' Cd strip inserted in test void.

X. Remark IX with a 0.030" thick, 3" x 4' Cd strip inserted in test void.

XI. Reflected on 2 sides. No end reflectors.

XII. Reflected on 4 sides. No end reflectors.

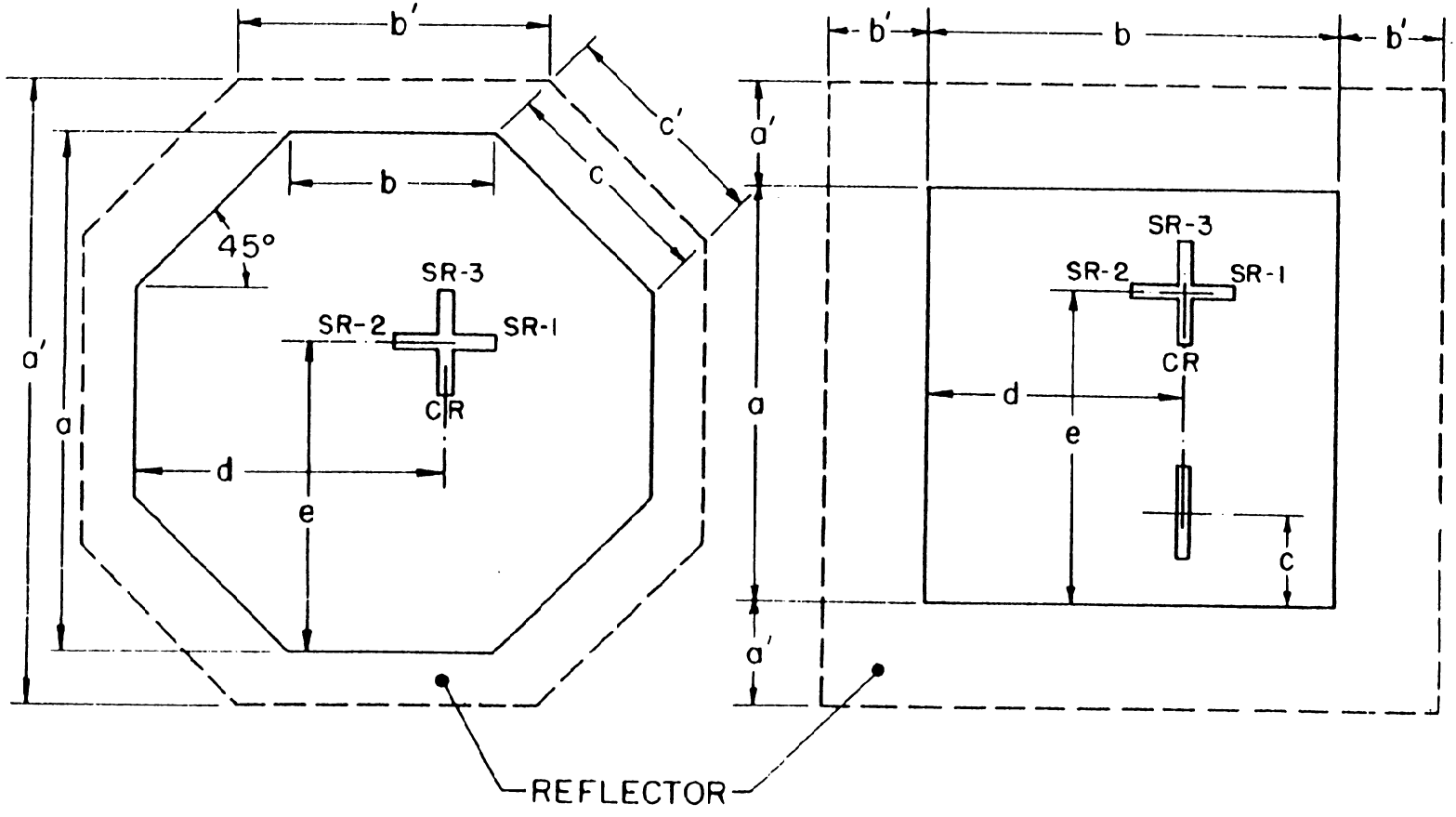

Fig. 10. Shapes and dimensions of test geometries. (See Table III).

V. CORRECTION OF DATA FOR SYSTEMATIC ERRORS

The physical model is a bare homogeneous graphite-oralloy system. Departures from this model are necessary in order to actually carry out the associated experimental program. The major departures are: the fuel is lumped into foils instead of being homogeneously distributed; gaps have to be provided for the safety and control rods required for safe operation; the actual system must be located in a vault or test cell and rest on a support table. To estimate the influence these experimental modifications have on system reactivity, a series of auxiliary experiments have been carried out.

The graphite moderator is in the form of 6" x 6" x 1/2" blocks. For convenience in stacking, two types of blocks are used; one at full graphite density, $\rho = 1.70$ g/cm^2; the other with slots milled out, $\rho = 1.03$ g/cm^2. In the lower density blocks, the milled slots allow the use of a lifting mechanism. Thus a stack is composed of a bottom low-density block and 11 high-density blocks above. The entire stack of 12 blocks is lifted at once with the lifting tool. The most straightforward method of building up the reactor is with entire horizontal planes of low-density blocks appearing every 6 inches in height. To test whether these planes caused neutron streaming, one assembly was reloaded with the low-density blocks randomized so that no horizontal low-density plane existed. The critical height decreased by less than 0.1 inch, which must be considered within experimental precision. Compare assemblies 7 and 8 in Table III.

Neutron reflection from the test-cell walls and floor was investigated by surrounding a critical system by low-energy-neutron-absorbing boral sheet. The capture of these returning neutrons before they entered the reactor increased the critical height approximately 0.1 inch. Compare assemblies 7 and 9 in Table III.

Aluminum guides in control and safety rod voids have a negligible effect on system reactivity. This was established by inserting extra aluminum in the safety-rod voids and observing no change in the system critical height. Compare assemblies 13 and 14 in Table III.

Critical Height Precision: The gross height increment is 1/2 inch, since this is the block thickness and changes are made by entire layers. However, extrapolations to critical with the data from four separate detection channels are consistent within 0.1 inch. Critical heights are quoted for all safety and control rods out of the core.

The subject of the conversion of data on systems with lumped fuel foils to equivalent homogeneously loaded systems is covered in Appendix I. The corrections deduced there are incorporated in the final data of this report. They can be summarized as follows:

C/U Absolute	Foil Thickness	Disadvantage Factor	C/U Effective
600	2.08 mils	0.889	675
1200	2.08 "	0.870	1379
2340	1.06 "	0.905	2586

VI. REDUCTION OF DATA TO AN IDEALIZED SYSTEM AND CORRESPONDING CRITICAL BUCKLINGS

A. Uncorrected Bucklings

ρ graphite = 1.645 excluding cross void

δ = 1.92 cm = extrapolation distance

A formula for the relation between the buckling of a regular octagon and a circle of equal area has been derived: See Appendix II.

$$B^2_{oct.} = 1.009\, B^2_{circle.}$$

Using this and the usual formula for buckling of a cylinder, one obtains for the 600/1 octagons

Octagon	H_c	$B^2_{obs.}$
48.5"	42.3"	20.96×10^{-4}
54.5"	38.8"	20.99×10^{-4}
60.5"	33.8"	21.26×10^{-4}

For the bare rectangular parallelepipeds, 48-1/2" x 48-1/2" square, one obtains the following values if the entire system (void plus graphite) is considered as homogeneous. The graphite density is then $\bar{\rho}$ = 1.636.

$C/U_{eff.}$	H_c	B^2_{axial}	$B^2_{obs.}$
675	40.0	8.88×10^{-4}	21.11×10^{-4}
1379	42.4	7.98×10^{-4}	20.17×10^{-4}
2586	47.6	6.34×10^{-4}	18.57×10^{-4}

B. Corrected Bucklings

The above bucklings ignore the effect of the control system cross void. The effect of this void was determined three ways.

1. The changes in critical height as the center of the cross was moved 12" and 18" off center were measured. See assemblies 7, 11, 12 and 19, 20, 21 in Table III. Extrapolation to the center of the cross just on the edge of the core gives a percentage change in height of:

3.1% for 1200/1 $\quad \Delta H_c = 1.3"$

3.3% for 2340/1 $\quad \Delta H_c = 1.6"$.

If we assume an average decrease of 3.2% in critical height as the effect of removing the cross void, new bucklings can be calculated. These are given in Table V. The corrected bucklings in Table V refer to systems with an average graphite density $\rho = 1.645 \frac{gm}{cm^3}$, as we have effectively removed the void.

Table V.

$(C/U)_{eff}$	Observed		Correction by extrapolation of cross motion		Correction by ϕ^2 perturbation		Correction by 2-group perturbation		Correction by doubling void effect	
	H_c	B^2	H_c	B^2	H_c	B^2	H_c	B^2	H_c	B^2
675	40.0	21.11×10^{-4}	38.7	21.69	39.0	21.53	38.8	21.64	-	-
1379	42.3	20.17×10^{-4}	41.0	20.69	41.2	20.62	41.0	20.69	40.2	21.03
2586	47.6	18.57×10^{-4}	46.1	18.98	46.1	18.98	45.9	19.04	45.4	19.18

An experiment was done on the 1200/1 system in which the full cross void was placed 18" from the center and an additional 1/2 cross void was placed at the center (assemblies No. 12 and 13). The increase in H_c associated with the half cross void was 0.9". If one assumes that the full cross effect is just double the half cross effect, one arrives at a $\Delta H_c = 1.8"$ for the full cross in the center. This $\Delta H_c = 1.8"$ is to be compared with the $\Delta H_c = 1.3"$ above arrived at by extrapolation. The agreement is poor. Effects of a test void, having half the volume of the control system,

were found for C/U = 1200 and 2340 systems with the control system 18" off center. The test void is then symmetrically opposite the control system. Assuming full cross effect to be double the half cross effect, the critical heights and B^2's listed in Table V are found.

2. Consider the cross void as a unit perturbation, δ, on the critical buckling, which we weight at various positions by the flux squared.

$$B^2_{\text{observed}} = B^2_o - \phi^2 \delta,$$

where B^2_o is the buckling without the cross-void perturbation. Substituting the observed bucklings for the three cross-void positions in this equation, and solving for the best values of δ and B^2_o, one obtains

1200/1	$\delta = 0.48 \times 10^{-4}$	$B^2_o = 20.62 \times 10^{-4}$
2340/1	$\delta = 0.41 \times 10^{-4}$	$B^2_o = 18.97 \times 10^{-4}$.

Both values of B^2 represent a 2% increase in the critical buckling for removal of the cross void. These values are included in Table V.

3. 2-group perturbation treatment: A slightly more sophisticated treatment involves the use of 2-group perturbation theory. The steps followed are:

a. Adjust the 2-group constants to give k = 1 for observed B^2.

b. Calculate $\delta k/k$ for the perturbation caused by the cross void in center. The effect of the void is considered as a reduction in density of the central 12" x 12" section of core graphite.

Thermal flux = alpha x fast flux

$\phi th = a \times \phi$

$$\frac{\Delta k}{k} = \left[\int \eta\Sigma_u \; a \; \phi^2 \, dv\right]^{-1} \left\{\int_v \phi^2 \, dv \left[\delta(p \; \Sigma_1 a) + \delta(\eta\Sigma_u)a - \delta(a^2 \; \Sigma_2) - \delta(\Sigma_1)\right] - \int_v (\nabla \phi)^2 \, a(D_1 + D_2) \, dv\right\} .$$

c. Relate $\delta k/k$ to the change in buckling using age theory.

The results of this calculation are also given in Table V.

C. Comparison With Modified Fermi Age Theory

The probability of a neutron escaping capture by U^{235} in slowing down is relatively small for the fuel-rich system C/U = 675, but gets progressively better as the fuel becomes more dilute. The Fermi Age equation for a graphite-moderated system in which the neutrons are captured at thermal energies is:

$$k = \frac{k\infty\, e^{-\tau B^2}}{1 + L^2 B^2} \qquad \text{where } \tau \text{ is computed down to thermal energy } \tau(E_o,\ E_{th}). \qquad (1)$$

Another formulation utilizing the Fermi slowing down model is to assume that no neutrons reach thermal energy but all neutrons are captured at some single higher energy E_i. Then

$$k = k\infty\, e^{-\tau(E_o,\ E_i)B^2}. \qquad (2)$$

TABLE VI

$(C/U)_{eff}$	B^2 at ρ=1.645	E_i (ev)	$\tau(E_o, E_i)$	$k\infty$	$k=k\infty\, e^{-\tau(E_o,\ E_i)B^2}$	$\frac{k=k\infty\, e^{-\tau(E_o,\ E_{th})B^2}}{1 + L^2 B^2}$
675	21.64×10^{-4}	0.15	313.6	1.98	1.006	0.931
1379	20.68	0.11	318.1	1.99	1.033	0.948
2586	19.04	0.09	321.1	1.97	1.071	0.962

This average capture energy E_i can be chosen to correspond with the average capture cross section in our self-shielding oralloy foils. Table VI shows that for the fuel-rich system C/U = 675, the modified Fermi age equation (2) works very well but gets progressively worse as the fuel becomes more dilute. This is reasonable because our assumption of no thermal neutrons becomes increasingly bad. On the other hand, worse results are obtained if we use the thermal-energy model (1).

Another simple model can be constructed by combining the two simple models above. The probability of a neutron reaching thermal energy can be considered as one minus the probability of being captured in U^{235} during slowing down. We can then assume that all neutrons captured during

slowing down are captured at our previous energy E_i. We then have two types of neutron captures and combine the k's, weighting by the respective number of neutrons.

p = prob of reaching thermal energy in ∞ medium

$$k = (1-p)k\infty(E_i)\, e^{-\tau(E_i)B^2} + p\, k\infty(E_{th})\, \frac{e^{-\tau(E_{th})B^2}}{1 + L^2 B^2} .$$

C/U	p using $\int \sigma_{235} \frac{dE}{E}$ = 1345b	k
675	0.0723	1.000
1379	0.2764	1.009
2586	0.5037	1.016

APPENDIX I

SELF-SHIELDING

The reactor systems whose critical parameters are to be determined are homogeneous mixtures of fuel and moderator, in this case oralloy and graphite. The physical approximation that has been made to this model consists of alternate layers of fuel foils and moderator plates. This fuel lumping results in two interrelated effects: a fine structure modification to the spatial flux distribution with a periodicity determined by the fuel foil spacing in the lattice, and a self-shielding effect within the fuel foil itself. The fine structure imposed on the flux distribution is measurably small and its effect on system reactivity is to first order negligible. The fuel atom self-shielding within the fuel foil is, on the other hand, a relatively large effect and must be corrected for.

On the basis of first-collision theory, a simple determination of the self-shielding factor for monoenergetic neutrons incident upon regular geometrical shapes with an isotropic angular distribution can be made.[1] For a purely absorbing infinite slab of thickness u in mean free paths, the disadvantage factor is:[2]

$$D.F. = \frac{1}{2u}\left[1 + (u-1)e^{-u} - u^2\int_u^\infty e^{-y}\,\frac{dy}{y}\right].$$

The disadvantage factor times the actual atomic absorption cross section is equal to the average effective absorption cross section for the fuel. Or, the equivalent amount of fuel in the desired homogeneous system is equal to the disadvantage factor times the actual amount of fuel in our lumped fuel system.

---

1 W.J.C. Bartels, Self-absorption of Monoenergetic Neutrons, KAPL-336, (1950).

2 National Defense Research Committee, Applied Mathematics Panel, Table of the Integral That Appears in The Evaluation of the Disadvantage Factor, Report No. AM-509, (1943); also, G. Placzek, The functions $E_n(x) = \int_1^\infty e^{-xu} u^{-n}\,du$, National Research Council of Canada Report No. MT-1.

$$\therefore (C/U)_{effective} = \frac{(C/U)_{nominal}}{D.F.\ (fuel\ foil)}.$$

To determine experimentally the D.F. for the fuel foils, small oralloy foils of different thicknesses were irradiated in a uniform neutron flux region in the critical assembly of interest. The capture of neutrons in the fuel results in fissions whose fission fragments are mainly retained in the foils. Some of these fission fragments are γ-emitters and the γ-emission intensity was used as a measure of foil activation or absorption. The γ's are counted in a NaI scintillation spectrometer and the β's are shielded out. The foil specific activity per unit thickness is plotted vs the foil thickness, and this curve is extrapolated and normalized to 1 at zero thickness. This is the foil disadvantage factor vs foil thickness curve. By choosing a thickness corresponding to the fuel foils, the appropriate disadvantage factor to use can be determined. Before displaying these experimentally determined curves for systems of different fuel concentrations, a major correction to the raw counting data will be discussed.

The monitor foils are clean oralloy disks with no surface covering. Fission fragments have varying ranges in uranium and a fraction of them escape through the foil surface. The fraction of the fragments escaping to the total produced in the foil depends upon the foil thickness. Data by Segrè and Wiegand[3] has been approximately confirmed through the use of aluminum catcher foils. The observed activation is corrected by a factor derived from their data.

$$(Act)_{corrected} = \frac{T + 0.10}{T} (Act)_{observed},$$

where T is the foil thickness in mils.

The relative specific foil activations can be determined to a precision of $\pm 1\text{-}1/2\%$ although some of the data for earlier systems are considerably worse. The details of the counting system and data reduction will appear elsewhere.

---

[3] Segrè and Wiegand, Phys. Rev. 70, 808 (1946).

For a source of thermal neutrons, a reactor consisting of a small graphite-oralloy core heavily reflected by D_2O was used. The self-shielding or monitor foils were placed in the D_2O 16" from the core edge. Though highly moderated and yielding a cadmium ratio of approximately 100, these neutrons were not all truly thermal. The average excess energy is small and unknown, pending further experiments. This data is referred to as the "thermal" disadvantage factor curve (Fig. 11). The flux depression in the D_2O is somewhat different from that in the graphite, therefore the D.F. curve for thermal neutrons in graphite might differ from that shown in Fig. 11. Fortunately, the self-shielding effect is large compared with the flux depression effect, and so one can side-step a most knotty problem, i.e , does the experimentally determined D.F. curve correct only for self-shielding or does it include both the self-shielding and the flux depression effect? It is felt that the D.F. curves include both self-shielding and flux-depression corrections, although in some cases only a partial correction is made for the flux depression. Since the systems are comparatively fuel rich, the thermal utilization is very nearly unity despite small flux depressions. This is one of the reasons why the above question can be answered either way without making a significant difference in the deduced equivalent fuel loading.

The fuel foils are 5-1/4" x 5-1/4" as compared with the graphite moderator blocks which are 6" x 6". Thus the fuel forms a three-dimensional lattice in the graphite moderator rather than the simpler one-dimensional systems of fuel sheets separated by graphite indicated earlier. The flux depression in the plane of the fuel foils is greater than that in the transverse plane. Relative flux values are shown in the fuel-foil plane in Fig. 12. The activations have been divided by the expected $\cos\left[(\pi/2)(x/x_o)\right]$ distribution. The maxima correspond to the points midway between the foils and the minima correspond to the midpoints of the foils. Near the edge of the reactor the flux rises abruptly due to the inadequacy of diffusion theory near a boundary. Near the center of the reactor the flux rise is associated with the lowered fuel concentration due to the structural modifications occasioned by the control and safety rod systems. It is seen that the amplitude of the flux oscillation is small in the plane of the fuel foils. In the transverse direction the amplitude is smaller, and when

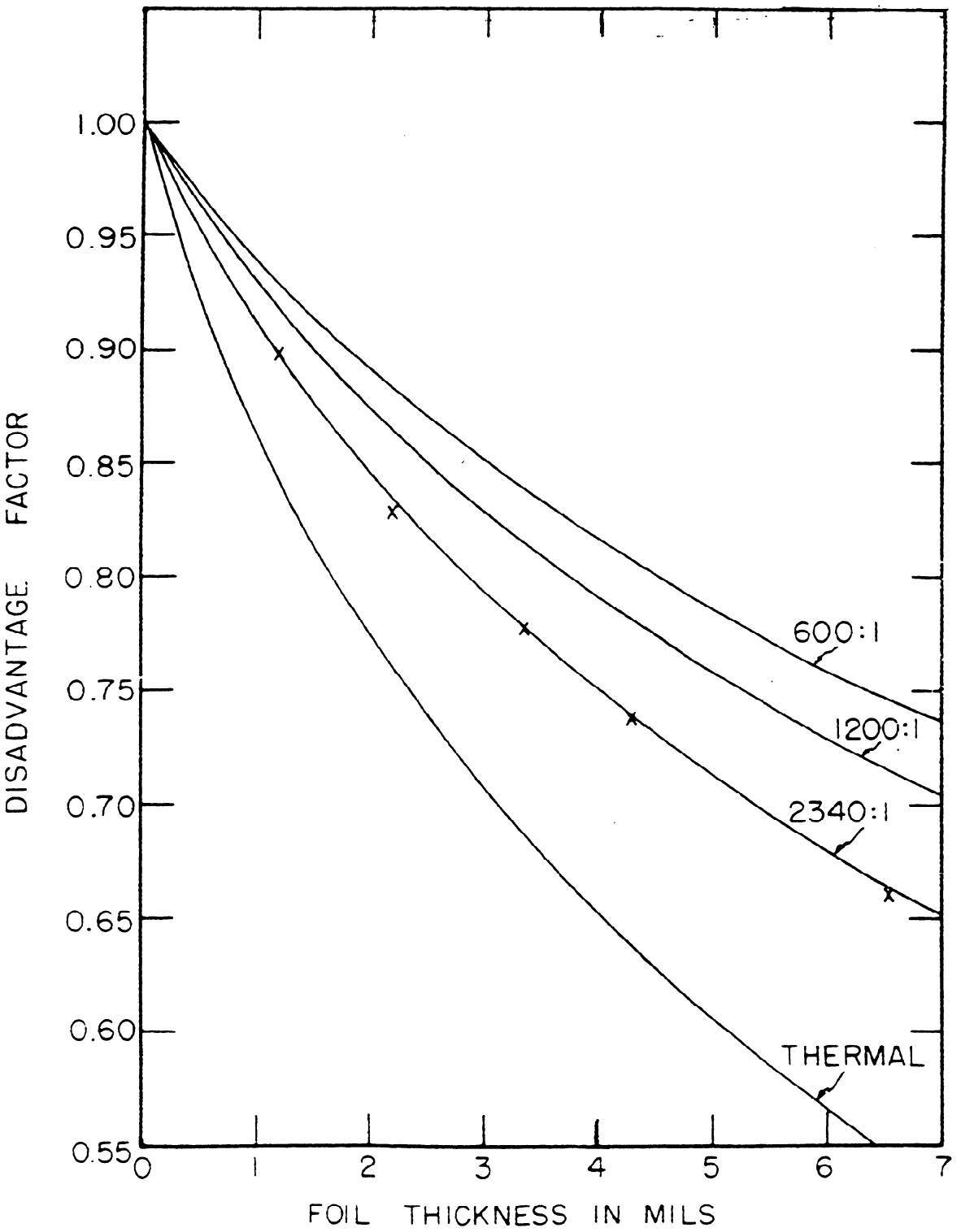

Fig. 11. Disadvantage factor vs uranium foil thickness.

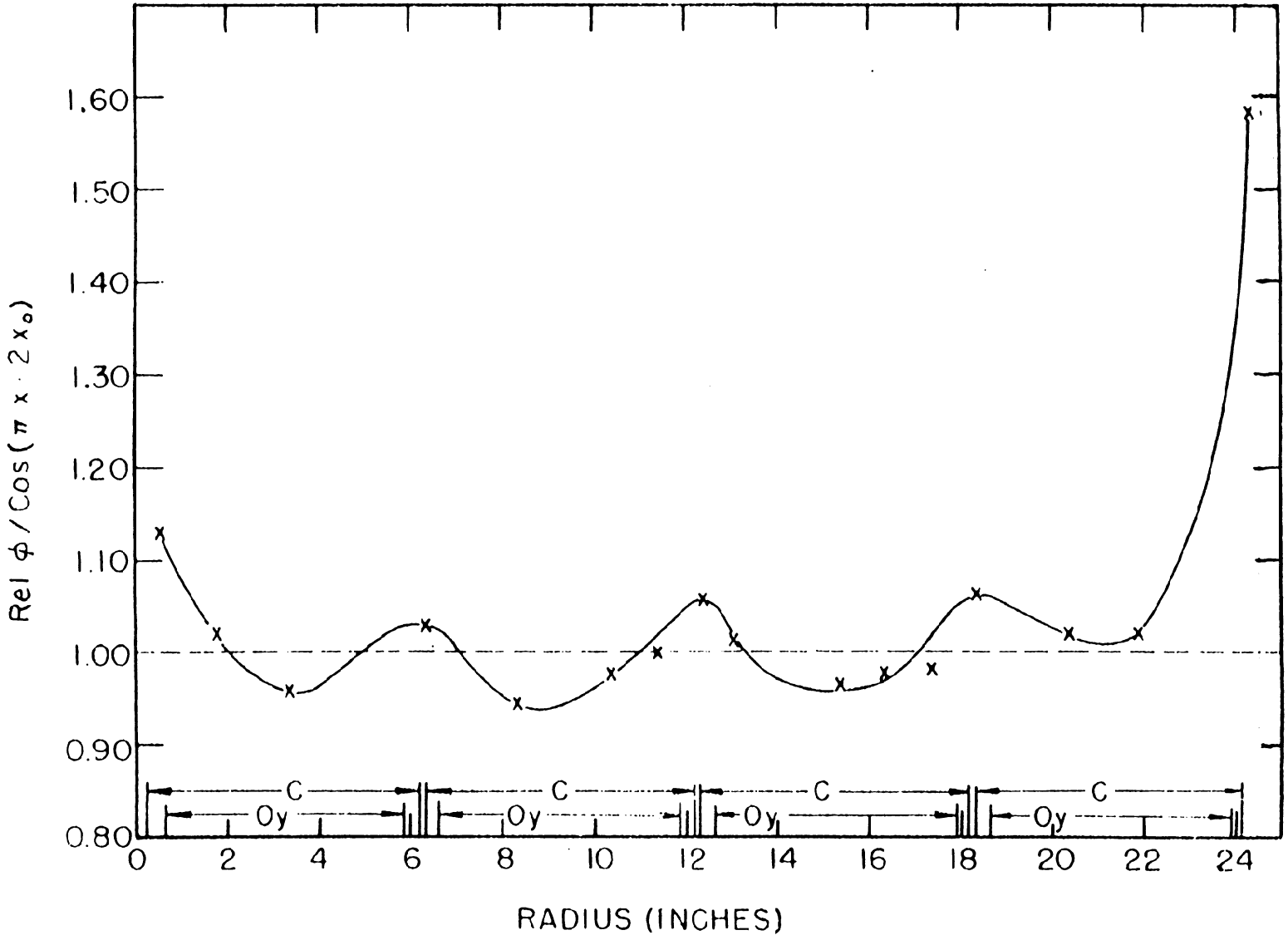

Fig. 12. Flux traverse in the plane of uranium foils.

this oscillation is translated into a change in equivalent fuel loading, the change is second order and negligible.

Figure 11 displays the disadvantage factor curves for the D_2O system and graphite/oralloy systems with $(C/U)_{nominal}$ of 600:1, 1200:1, 2340:1. The following table lists the $(C/U)_{nominal}$, fuel foil thickness, D.F. and $(C/U)_{eff.}$ This $(C/U)_{effective}$ is the C/U that would be required to make a homogeneously loaded system (oralloy, graphite of $\overline{\rho}$ = 1.63) of the same size critical.

$(C/U)_{nominal}$	Fuel foil thickness (mils)	D.F.	$(C/U)_{effective}$
$(C/U)_{test\ assembly}$	2.08	0.768	1.302 $(C/U)_{test\ assembly}$
600	2.08	0.889	675
1200	2.08	0.870	1379
2340	1.06	0.905	2586

APPENDIX II

GEOMETRICAL BUCKLING OF A REGULAR OCTAGON

The method described here is applicable to any regular polygon - for generality, therefore, it is developed for a regular polygon of n sides and then specialized to the octagon. To obtain the buckling B^2, it is necessary to solve the equation

$$\nabla^2\phi + B^2\phi = 0,$$

and subject the solution to the appropriate boundary conditions. The method described here is only concerned with the solution inside the region indicated in the diagram, which indicates the geometry of the system.

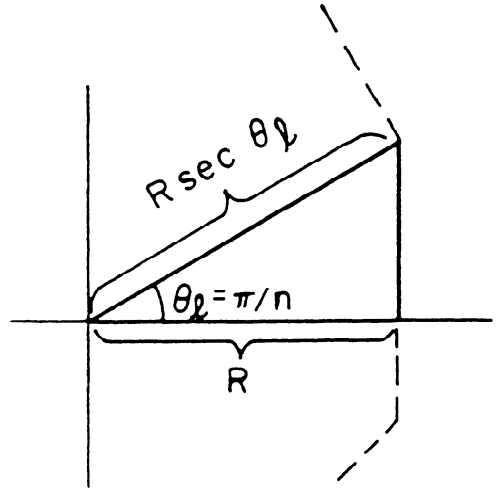

Expressing the Laplacian in cylindrical coordinates the equation is:

$$\frac{\partial^2\phi}{\partial r^2} + \frac{1}{r}\frac{\partial\phi}{\partial r} + \frac{1}{r^2}\frac{\partial^2\phi}{\partial\theta^2} + \frac{\partial^2\phi}{\partial z^2} + B^2\phi = 0.$$

The solution is separable in the three coordinates; therefore it is fairly simple to show that

$$\phi(r, \theta, z) = A_k J_{\nu_k}(B' r) \cos \nu_k\theta \cos \beta z,$$

where A_k is an arbitrary constant and

$\nu_k = nk$ $\quad k = 0, 1, 2, \text{----}$

$B' = \sqrt{B^2 - \beta^2}$

$\beta = (\pi/H)$, where H is the extrapolated height.

Three boundary conditions have already been invoked to obtain this result. They are:

(1) $\phi\ (r,\ \theta,\ \pm H/2) = 0$

(2) $\partial\phi/\partial\theta = 0$ for $\theta = 0$, all r, all z.

(3) $\partial\phi/\partial\theta = 0$ for $\theta = \theta_\ell$, all r, all z.

One final boundary condition has yet to be satisfied:

(4) $\phi\ (R \sec\theta,\ \theta,\ z) = 0$ for $0 \leq \theta \leq \theta_\ell$.

Clearly this requires a linear combination of the above solutions. That is:

$$\phi\ (r,\ \theta,\ z) = \sum_{k=0}^{\infty} A_k J_{\nu_k} (B' r) \cos \nu_k\theta \cos\beta z.$$

Thus, B.C. No. 4 becomes:

$$\sum_{k=0}^{\infty} A_k J_{\nu_k} (B' R \sec\theta) \cos \nu_k\theta = 0. \qquad 0 \leq \theta \leq \theta_\ell$$

This represents a system of infinitely many equations (one such equation for each value of θ in the interval), each containing infinitely many terms ($k = 0, 1, 2 \ldots$). For practical calculations, this system of equations is approximated by a finite system. This is done by requiring that the flux vanish only for a finite number $(m + 1)$ of values θ_j of θ in the interval $0 \leq \theta \leq \theta_\ell$. For convenience, the θ_j are taken to be evenly spaced:

$$\theta_j = j\,\theta_\ell/m = \frac{j\,\pi}{mn} \qquad j = 0, 1, \ldots m.$$

The above system is thus replaced by

$$\sum_{k=0}^{m} A_k J_{\nu_k} (B' R \sec\theta_j) \cos \nu_k\,\theta_j = 0. \quad j = 0, 1 \ldots m.$$

The condition for nontrivial solutions for the A_k is that the determinant of the coefficients vanishes.

$$\left| C_{kj} \right| = 0$$

$$C_{kj} = J_{\nu_k} (B' R \sec\theta_j) \cos \nu_k\theta_j.$$

This determinantal equation may be solved for B'R. Of course, there will be a multiplicity of solutions and an additional criterion is required to decide which is the correct root. This criterion is provided by comparing the buckling B'2 of the polygon with that of a circle of equal area (B_c^2), and with that of the inscribed circle (B_{ic}^2). Clearly:

$$B_c^2 < B'^2 < B_{ic}^2,$$

and this is equivalent to

$$2.34152 < B'R < 2.4048 .$$

The above equation has been solved for an octagonal cross section (n = 8) in the m = 1, 2, and 3 approximation.
The results were:

$$\begin{aligned} B'R &= 2.339 \qquad m = 1 \\ &= 2.350 \qquad m = 2 \\ &= 2.3518 \qquad m = 3 \end{aligned}$$

Hence $B'^2 = 1.0088\, B_c^2$ where, again, B_c^2 is the geometrical buckling of a circle with the same cross-sectional area as the octagon.

/cd